www.vbripress.com/aml, DOI: 10.5185/amlett.2016.6112 Published online by the VBRI Press in 2016

Study of ball milled bismuth telluride composites reinforced with MWCNTs for thermoelectric behaviour

Sandeep K. Pundir[1,2*], Sukhvir Singh[1], B. Sivaiah[1], Rajesh Kumar[2], Ajay Dhar[1]

[1]*Electron and Ion Microscopy Division, CSIR-National Physical Laboratory, New Delhi 110012, India*
[2]*Department of Physics, Punjab University, Chandigarh 160014, India*

[*]Corresponding author. Tel: (+91) 11-45608394; Email: skpnagali@gmail.com

Received: 26 August 2015, Revised: 04 February 2016 and Accepted: 20 May 2016

ABSTRACT

Thermoelectric properties of n-type bismuth telluride and its nanocomposite reinforced with different concentration of multi wall carbon nanotubes (MWCNTs) are reported. Nanocomposites of bismuth telluride with MWCNTs were synthesized by using high energy ball milling followed by spark plasma sintering (SPS). MWCNTs reinforced nanocomposites of bismuth telluride resulted improvement in its figure of merit ZT from 0.76 (for Bi_2Te_3) to 0.85 (for Bi_2Te_3 + 2%MWCNTs) at 473K temperature. Thermoelectric parameters of nanocomposites of Bi_2Te_3 were characterized by Laser Flash Technique. The improvements found in ZT value may be due to decrease in thermal conductivity of the nanocomposites. Concentration of MWCNTs in bismuth telluride leads to dampening the phonon propagation with addition to the interface scattering of phonons from phase boundaries as well as grain boundaries which leads to decrease in thermal conductivity. Copyright © 2016 VBRI Press.

Keywords: Ball milling; bismuth telluride; microstructure; spark plasma sintering; thermoelectric properties.

Introduction

Among thermoelectric materials bismuth telluride based device are widely used in many potential applications such as for the fabrication of thermal sensors, laser diodes, thermoelectric refrigeration for cooling and power generation [**1-3**]. Also applications include Peltier coolers for refrigeration in various microelectronic devices and thermal management of electronic and optical components, and thermopiles for direct conversion of thermal to electrical energy from waste-heat and ambient thermal sources [**4-6**]. Efficiency of the thermoelectric material is determined by the figure of merit $ZT = S^2\sigma T/k$ [**7**]. Where, ZT = Figure of merit, S = Seebeck's Coefficient or thermoelectric power, σ = electrical conductivity, T=Temperature and k= thermal conductivity. In order to increase the thermoelectric efficiency of the material we need to improve the figure of merit. The figure of merit can be increased by increasing electrical conductivity, improving thermoelectric Power and reducing thermal conductivity. Recently researchers are focusing on reducing the thermal conductivity [**8, 9**]. Carriers responsible for the conduction of heat in the material are mainly electrons and phonons. However, electrons contribution for thermal conductivity is small enough so that we need to suppress phonon conductivity rather than reducing thermal conductivity due to electrons. One of the best methods to reduce phonon conductivity is by increasing the number of interfaces encountered by the phonons in the material [**10-12**]. This can be done as follows: (1) Using nanoparticles of Bi_2Te_3. (2) By incorporating nano structured materials in the matrix. Bulk material made by compressing the nanoparticle will offer increased interface in the path of the phonons. Addition of foreign nanostructure materials also increases the interface.

MWCNTs play a very important role in reducing the thermal conductivity of bismuth telluride based nanocomposites [**13, 14**]. The experimentally measured thermal conductivity of an individual multi-wall CNT (MWCNT) was found to be 3000 $Wm^{-1}K^{-1}$ while, for aligned MWCNTs samples was found to be in the range of 12 to 17 $Wm^{-1}K^{-1}$ [**15**]. Therefore, it implies that by proper engineering and nanostructuring of the materials, thermal conductivity can be controlled. Beside this CNTs exhibit extraordinary strength and high electrical conductivity, and have efficient lower thermal conductivity when uses in thermoelectric based nanocomposites [**12**]. In the literature it is found that due to ball milling destruction in CNTs occurs [**16**], and corresponding reduction in the intensity of the peak of G-band and D-band of MWCNTs observed in Raman spectra. Reduction of the G-band intensity clearly reveals that ball mill is causing a defect in MWCNTs and reduction in D-band shows the complete destruction of MWCNT structure. These defective MWCNTs do not show the property shown by ideal MWCNTs.

So excessive ball milling of MWCNTs is always undesirable. Keeping in view of the importance and application, we have made an attempt to synthesize bismuth telluride with different weight percent of MWCNTs. In the present study, excessive ball milling has been avoided and

only 4hr ball milling was preferred to observe the effect of reinforcement of MWCNTs on thermoelectric parameters.

Experimental

Material synthesis

Bi_2Te_3 bulk compound was synthesized by using vertical directional solidifications VDS method [**6**]. A small piece was taken from the as synthesized Bi_2Te_3 bulk compound and ground manually in the astle to form powder. This manually ground Bi_2Te_3 powder was further ball milled with different weight percentage of MWCNTs (*i.e.* 1.5%, 2%, 2.5%, and 3% by weight). Ball milling of the composites were carried out at the rate of 180 rpm for 4 hrs in Ar atmosphere to obtain fine powder. After ball milling, spark plasma sintering was carried out at 673K temperature and pressure of 7.5 kN/m^2 for 12 minutes. To study the thermoelectric properties a disk of 12.7 mm in diameter and 2 mm in thickness was prepared from SPS machine using graphite dies. A cuboid of 2 × 2 × 10 mm was cut and polished from the disk and used for electrical conductivity and Seebeck Coefficient measurements. Microstructural and crystallographic characterization was carried out by scanning electrons microscope (SEM), high resolution transmission electrons microscope (HRTEM) and XRD, respectively. Thermoelectric parameters such as Seebeck Coefficient, electrical conductivity, thermal diffusivity, of the samples were determined by using Laser Flash Technique.

Characterizations

Phase identification, crystalline structures and lattice parameters were investigated by X-ray diffractometer, model: D8 Advance, Bruker-AXS before and after SPS. Surface morphology and elemental analysis were carried by using scanning electron microscopy (SEM) model EVOMA10 and energy dispersive spectroscope (EDS) model INCA250 respectively, attach with SEM. Internal microstructure, grain size, shape, structures and crystallographic orientations were investigated by using transmission electron microscope (TEM) model FEI G2 STWIN operated at 300kV. Carrier concentration type and density of the pellets were determined by using p-n type tester and Archimedes kit, respectively. Thermoelectric parameters such as Seebeck Coefficient, electrical conductivity, and thermal diffusivity were determined by using Laser Flash Technique model: Linseis, LFA 1000 and Ulvac-Riko ZEM-3, respectively. Thermal conductivity of the pellets was calculated by using the relation, $k=\alpha\rho Cp$, where, α thermal diffusivity, ρ density of the pellets and Cp specific heat of the material. Specific heat of the pellets was measured by differential scanning calorimeter (DSC). Figure of merit (ZT) was calculated by using the value of electrical conductivity, Seebeck coefficient and thermal conductivity.

Results and discussion

Fig. 1(a) shows the XRD pattern of 4 hrs ball milled Bi_2Te_3 powder and its composite with 1.5%, 2%, 2.5% and 3% (by wt) MWCNTs before SPS. XRD data recorded at room temperature was indexed thoroughly and confirm that all the reflections were found to be in good agreement with the standard values of JCPDS file No. 82-0358 of Bi_2Te_3. XRD pattern indicates the formation of single phase Bi_2Te_3 compound having rhombohedral structure. **Fig. 1(b)** shows XRD pattern of 4hr ball milled Bi_2Te_3 and its composite with 1.5%, 2%, 2.5% and 3% (by wt) MWCNTs after SPS. From the XRD pattern it is observed that the intensity of the XRD peaks increases after SPS. Increase in the intensity of the XRD peaks after SPS may be due to grain growth in the materials during SPS. Average crystallite size was calculated by Scherrer equation and found to be in the range 14 - 32 nm. It is also important to mention here that after SPS some new reflections in the XRD patterns are also observed, which indicate that some grain growth have taken place in the materials during SPS. However, we could not see any reflection of MWCNTs in XRD patterns. This may be due to lower concentration of the MWCNTs incorporated in the materials or MWCNTs have very lower count of intensity as compared to the Bi_2Te_3.

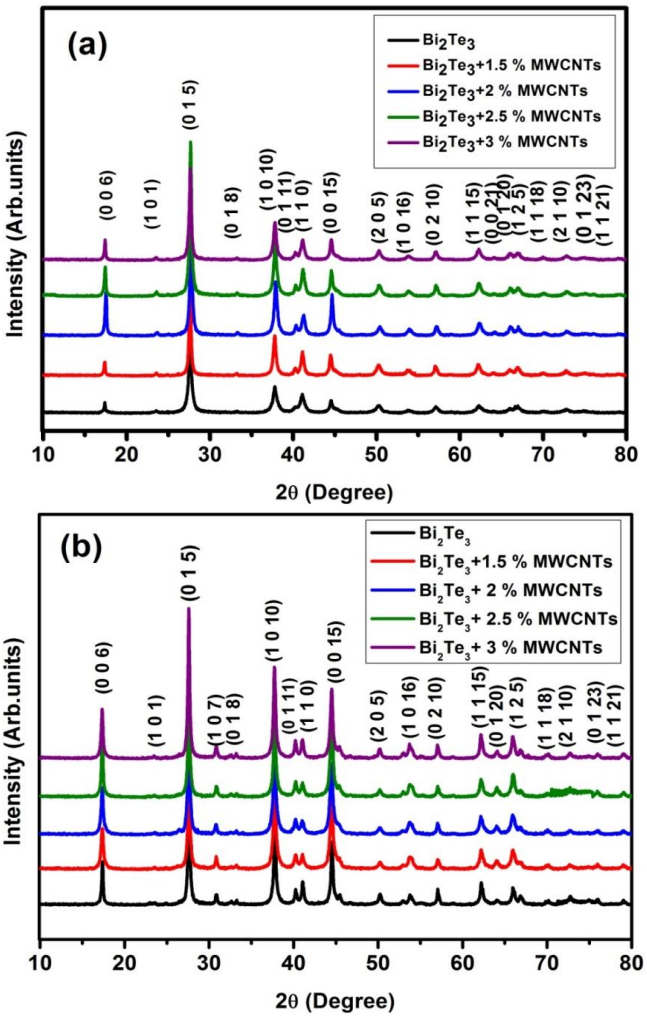

Fig. 1. (a) Shows the XRD patterns of 4 hrs ball mill powder reinforced by MWCNTs (b) XRD patterns of pellets after SPS at 473K temperature.

A small piece taken from the as synthesized pellets was scanned under SEM to investigate the surface microstructure of the composite. **Fig. 2(a)** shows the surface morphology of the broken piece taken from the pellet. It depicts the Bi_2Te_3 grains having platy and granular shape of particles and size varying between 200 nm to 1 µm. Surface morphology of the pellet revealed the

presence of nano pores and randomly distributed MWCNTs marked by arrows as shown in **Fig. 2**(a). SEM micrograph also revealed that MWCNTs is not uniformly distributed on the surface of the pellet. **Fig. 2**(b) depicts the energy dispersive spectroscopy (EDS) patterns of Bi_2Te_3 composite reinforced with MWCNTs. EDS pattern as shown in the **Fig. 2(b)** revealing the presence of carbon along with the Bi and Te elements. The presence of oxygen as revealed in the EDS spectra of the composite may be due to trapped oxygen in the micro and nano pores present in the composites.

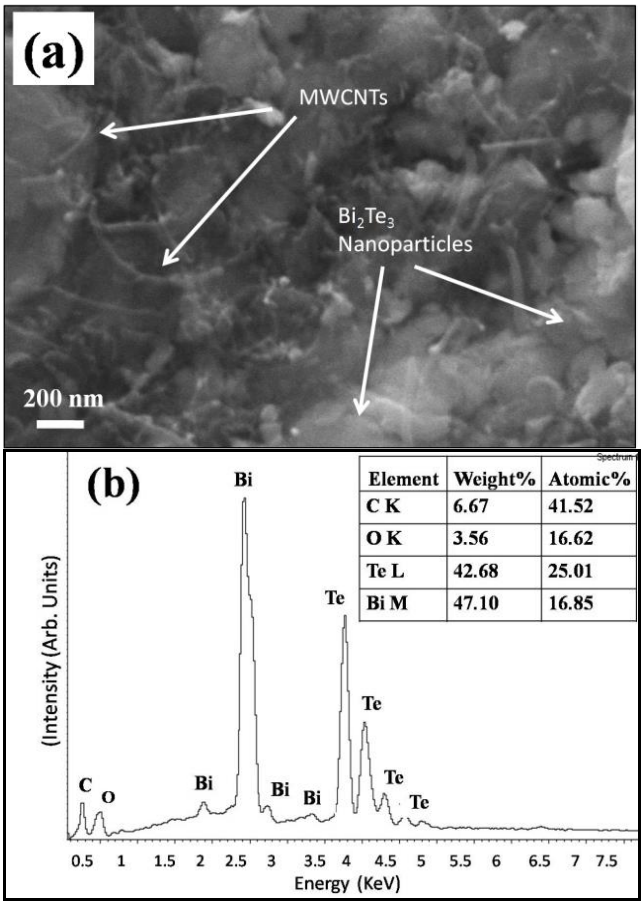

Fig. 2. (a) SEM image of top surface of pellet, (b) EDS spectra of the same area.

A detailed microstructural characterization was carried out by using transmission electron microscope (TEM) to examine the internal microstructure, phase transformation, crystallographic structure of ball milled Bi_2Te_3 composite reinforced with MWCNTs. **Fig. 3(a)** shows TEM image of Bi_2Te_3 composite revealing agglomeration of particles having sheet or platy like shape. MWCNTs are also seen bridging with Bi_2Te_3 particles as shown in the **Fig. 3(a)**. Selected area electron diffraction pattern (SAEDP) of the corresponding area revealed ring pattern indicating polycrystalline nature of the composite material. Detailed analysis of SAED ring pattern suggests that the planes of orientation (0 1 5), (1 0 10), (1 1 0), (2 0 5), (1 1 15), and (2 1 10) of Bi_2Te_3 are present which corresponds to rhombohedral structure.

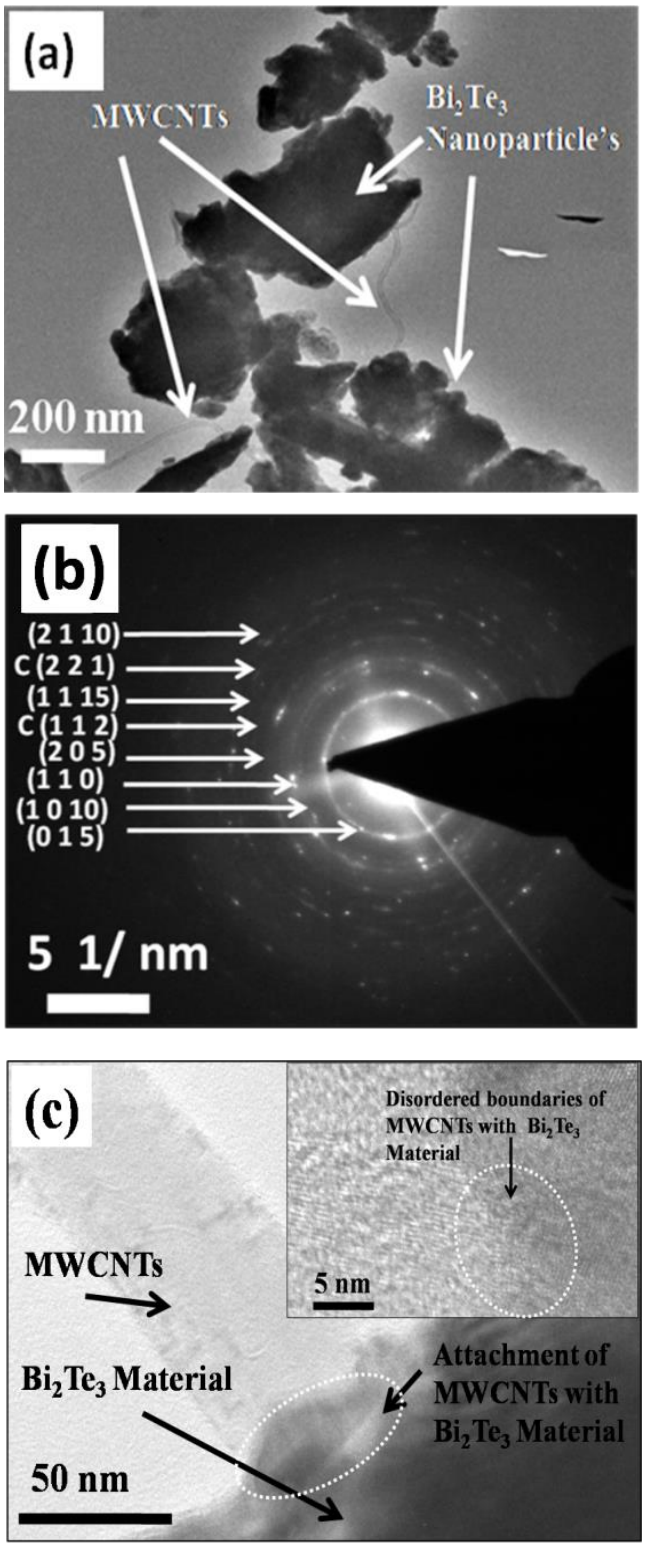

Fig. 3. (a) TEM image of Bi_2Te_3 composite shows the attachment of Bi_2Te_3 particle with MWCNTs (b) Represents the corresponding SAEDP of the composite and (c) shows the HRTEM micrograph depicting the disordered region at the junction of MWCNTs with Bi_2Te_3 particles.

The results of electron diffraction of Bi_2Te_3 are in good agreement with the JCPDS file No. (82-0358). Presence of MWCNTs in composite is also observed along (221) and (112) lattice planes as marked in SAEDP. This is important to mention here that these reflections were not observed in the XRD pattern. This is may be due to the fact that the ratio of scattering intensity of x-rays to that of electron is

about 1:106 consequently a very thin film, say several nanometer thickness can give sufficient intensity of diffracted electron to be easily recorded or observed. Since the scattering amplitude of an electron is much less dependent on atomic number unlike x-rays, the resolution of electron diffraction is much better. Hence the lighter atoms even in presence of the heavier one can be resolved by electron diffraction technique. In X-rays the heavier atom often masks the contribution of the lighter ones, thus the electron diffraction method is very powerful tool for the investigation of thin films and surface layers.

In **Fig. 3(c)** HRTEM micrograph of Bi_2Te_3 composite reinforced with MWCNTs has been shown and depicting the presence of MWCNTs with Bi_2Te_3 particles. It is observed from the HRTEM micrograph that MWCNTs make an attachment with Bi_2Te_3 particles and creates the disordered region at the junctions. This disordered junction would be responsible for decrease in thermal conductivity due to phonon scattering at the junction in the composites.

Raman spectroscopy has been widely used to investigate the physical and structural properties of carbon nanotubes (CNTs) and its application in CNT reinforced composites [17]. Raman scattering measurements were performed on Bi_2Te_3 and its composite reinforced with MWCNTs in the backscattering geometry using the Jobin-Yvon T64000 Triple-mate instrument coupled with the Ar+ 514.5nm laser line. A charge-coupled device system (CCD) with accuracy of 0.7 cm^{-1} was used to collect the scattered data. **Fig. 4(a)** shows the Raman spectra of MWCNTs, Bi_2Te_3 and Bi_2Te_3 nanocomposites reinforced with MWCNTs in different weight % in the spectral range from 50 cm^{-1} to 3000 cm^{-1}. While **Fig. 4(b)** shows the Raman spectra in the spectral range from 50 cm^{-1} to 300 cm^{-1}. In **Fig. 4(a)** three different peaks were observed in the Raman spectra of MWCNTs. Peak observed at 1350 cm^{-1} in MWCNTs Raman spectra corresponds to D band (defect mode), peak observed at 1580 cm^{-1} corresponds to G band (related to the tangential vibrations of the C atoms) and peak observed at 2700 cm^{-1} is corresponding to 2D second order band. Position of these peaks in the spectra confirms the MWCNTs [**18**]. It is observed from the **Fig. 4(a)** that peak at 1350 cm^{-1} is less intense in comparison to the G band peak at 1580 cm^{-1}. This elucidates the presence of defect concentration in CNTs such as deformation, wrinkles, and disordered crystalline structure. Broadening and lower intensity of second order defects (2D band) as compared to G bands in Raman spectra confirms the multivalve nature of the CNTs. It is to be noted that with increasing the weight percentage of MWCNTs in Bi_2Te_3 the intensity of composites in Raman peak corresponding to 1350 cm^{-1}, 1580 cm^{-1} and 2700 cm^{-1} are decreased as compared to the Raman spectra of pure MWCNTs. **Fig. 4(b)** depicts the Raman spectra of Bi_2Te_3 and its composites with MWCNTs. Three main peaks observed in the spectral range from 50 cm^{-1} to 300 cm^{-1} in the Raman spectra as shown in the **Fig. 4(b)**. These peaks observed at 92 cm^{-1}, 121 cm^{-1}, and 140 cm^{-1} in Raman spectra of Bi_2Te_3 and match with the values found in literature [**19, 20**].

Peak observed in Raman spectra at 121 cm^{-1} has highest intensity, while broadening in this peak gives information about crystalline structure of Bi_2Te_3. Also mixing of MWCNTs in Bi_2Te_3 is affecting the intensity and peak position. When the weight percent ratio of MWCNTs changes to 1.5% and 2% in Bi_2Te_3 the peak intensity corresponding to 121 cm^{-1} of Bi_2Te_3 is decreased and the position corresponding to the peak found to be shifted towards lower side. Interestingly at 2.5% mixing of MWCNTs in Bi_2Te_3 the peak corresponding to100 cm^{-1} is highly intense and the peak corresponding to 114 cm^{-1} is almost disappearing. When we further increase the weight percentage ratio to 3% all the three peak corresponding to 100 cm^{-1}, 114 cm^{-1}, and 138 cm^{-1} again appear in the Raman spectra. Raman spectra observed for 2.5% mixing of MWCNTs depicts unusual behaviour. This unusual behaviour observed in Raman spectra exactly not known right now but it is expected that it may be due to non uniform distribution of MWCNTs in the pellet sample.

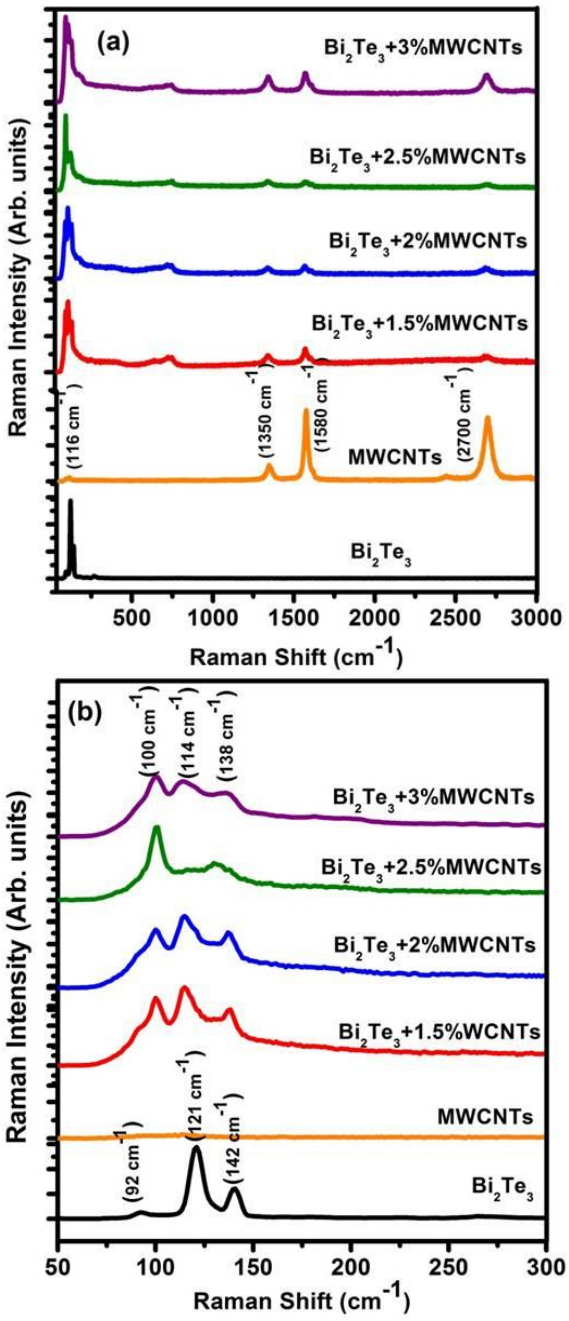

Fig. 4. (a) shows the Raman spectra of MWCNTs, Bi_2Te_3 and Bi_2Te_3 nanocomposite with different weight percentage of MWCNTs in the spectrum range 30 cm^{-1}- 3000 cm^{-1} and (b) shows the Raman spectra in the spectrum range 50 cm^{-1} – 300 cm^{-1}.

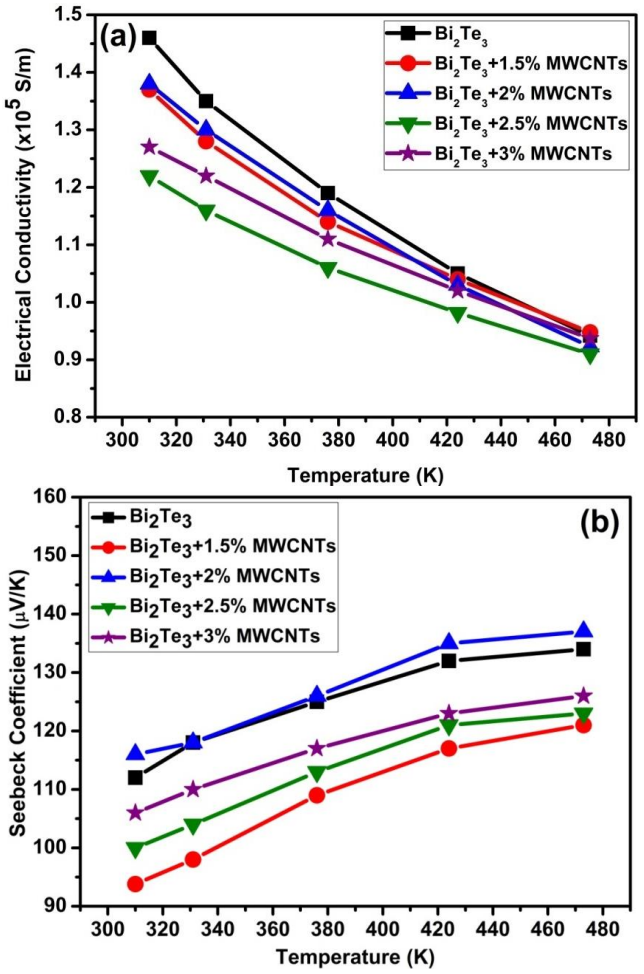

Fig. 5. (a) Depict the plot of variation in electrical conductivity with temperature for all the samples, and (b) Depict the plot of variation in Seebeck Coefficient with temperature for all the samples.

The thermoelectric parameters such as electrical conductivity, Seebeck Coefficient, thermal conductivity and figure of merit of 4 hrs ball milled Bi_2Te_3, and its composites with different weight percentage of MWCNTs determined by Laser Flash technique. **Fig. 5(a)** depicts the plot of variation in electrical conductivity with temperature of all the samples. It is observed from the graph that decreases in electrical conductivity with increase in temperature reveals the metallic behavior of the samples. By the mixing of MWCNTs in Bi_2Te_3 electrical conductivity found to be decreased as compared from Bi_2Te_3. As a result, addition of MWCNTs and ball milling decreases the electrical conductivity of the Bi_2Te_3 which may due to scattering of free carriers from the interface boundaries, which found to increase with the increase in the MWCNTs concentration in the Bi_2Te_3.

Fig. 5(b) represents the variation in Seebeck Coefficient with temperature of Bi_2Te_3 composites incorporated with MWCNTs. It is observed from the graph that Seebeck Coefficient of Bi_2Te_3+2%MWCNTs composites has highest value as compared to other compositions. With the temperature Seebeck Coefficient of all the samples increases as shown in the figure.

Fig. 6(a) represents the change in thermal conductivity as a function of temperature for Bi_2Te_3, and its composites with MWCNTs. From the **Fig. 6(a)** it is observed that the value of thermal conductivity decreases with increase in the weight percentage of MWCNTs in the Bi_2Te_3. Addition of MWCNTs in the ball milled Bi_2Te_3 creates more interfaces, defects and increase density of grain boundaries. Therefore, thermal conductivity of the Bi_2Te_3 composites decreases with addition of MWCNTs due to phonon scattering from the grain boundaries. This indicates that the lattice thermal conductivity has been efficiently restrained by addition MWCNTs and nano structuring by using ball milling, which enhances phonon-grain boundary scattering and results in a remarkable decrease in thermal conductivity.

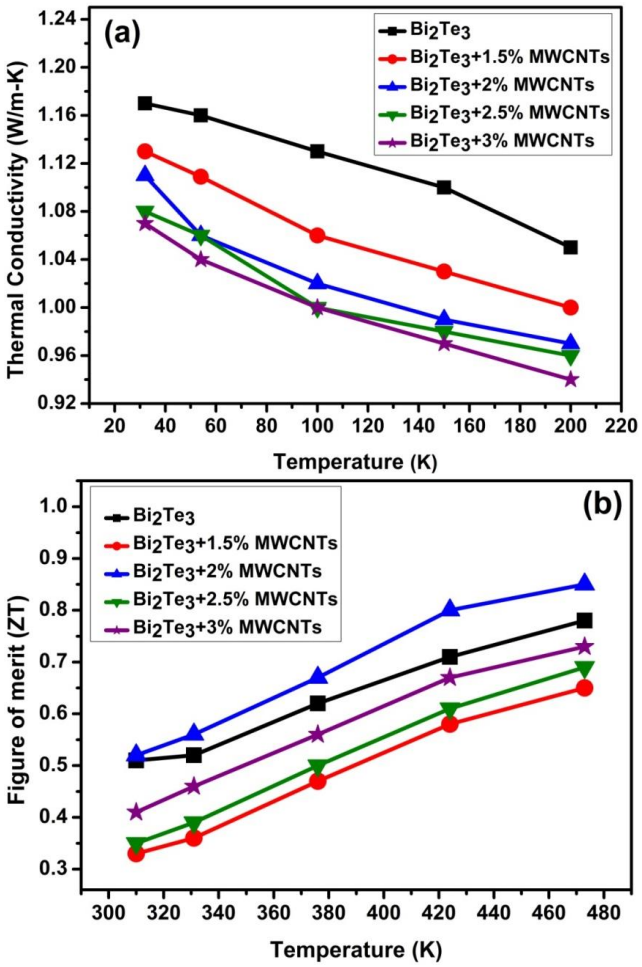

Fig. 6. (a) Depict the plot of variation in thermal conductivity with temperature and (b) Depict the plot of variation in figure of merit (ZT) with temperature.

Fig. 6(b) shows the variation in figure of merit (ZT) as a function of temperature. Figure of merit calculated by using as determined thermoelectric parameters such as electrical conductivity, Seebeck Coefficient, thermal conductivity. It is observed from the **Fig. 6(b)** that highest ZT (~0.85) has been observed for Bi_2Te_3 reinforced with 2% MWCNTs composite at 424K temperature, as compared to the Bi_2Te_3 (ZT~0.76), which is mainly due to decrease in thermal conductivity of the composites.

Conclusion

In conclusion, we have synthesized Bi_2Te_3 with different weight percentage of MWCNTs reinforced nanocomposite by ball milling process under Ar atmosphere. A noticeable variation in the thermoelectric parameters such as thermal

conductivity, Seebeck coefficient and the calculated figure of merit ZT have been observed. This study demonstrates that the thermal conductivity of the Bi_2Te_3 composite reinforced with MWCNTs is found to decrease and therefore ZT value found to improve for (2% wt) mixing of MWCNTs. These results are very encouraging and it is expected that it would be a promising thermoelectric material in future for commercial applications near room temperature for thermoelectric generation and other thermoelectric applications. Efforts are being made in order to achieve further higher ZT value by optimising the high energy ball milling and SPS process parameters and is in process.

Acknowledgements

This work has been carried out under CSIR-TAPSUN Network Project NWP-54. One of the authors Sandeep Kumar Pundir thanks to Director, CSIR-National Physical Laboratory, India for providing the necessary experimental facilities to carry out the research work.

Reference

1. Snyder, G.J.; Toberer, E.S.; *Nat. Mater.*, **2008,** 7, 105. **DOI:** 10.1038/nmat2090.
2. Pundir, S.K.; Singh, S.; Srivastava, A. K.; Dalai, M. K.; Kumar, R.; *Adv. Sci. Eng. and Med.*, **2013**, 5, 436. **DOI:** 10.1166/asem.2013.1274.
3. Ma, Y.; Hao, Q.; Poudel, B.; Lan, Y.; Yu, B.; Wang, D.; *Nano. Lett.*, **2008**, 8, 2580. **DOI:** 10.1021/nl8009928.
4. Fan, X.A.; Yang, J.Y.; Xie, Z.; Li, K.; Zhu, W.; Duan, X.K.; Xiao, C.J.; Zhang, Q.Q.; *J. Phys. D: Appl. Phys.*, **2007**, 40, 5975. **DOI:** 10.1088/0022-3727/40/19/029.
5. Chen, Z.G.; Hana, G.; Yang, L.; Cheng, L.; Zou, J.; *Prog. in Nat. Sci: Mater. Internat.*, **2012**, 22, 535. **DOI:** 10.1016/j.pnsc.2012.11.011.
6. Pundir, S.K.; Parveen, J.; Singh, S.; Srivastava, A.K.; Kumar, R.; *Adv Sci Eng and Med.*, **2014,** 6, 1006. **DOI:** 10.1166/asem.2014.1609.
7. Li, Z.; Zhao, G. L.; Zhang, P.; Guo, S.; Tang, J.; *Mater. Sci. and Appl*., **2012**, 3, 833. **DOI:** 10.1109/ICT.2002.1190350.
8. Takashiri, M.; Tanaka, S.; Hagino, H.; Miyazaki, K.; *J. Appl. Phys.*, **2012**, 112, 084315. **DOI:** DOI: 10.1063/1.4759326
9. Souza, S.M.; Trichês, D.M.; Poffo, C.M.; Lima, D.J.C.; Grandi, T.A.; Biasi, D.R.S.; *J. Appl. Phys.*, **2011**, 109, 013512. **DOI:** 10.1063/1.3520658.
10. Tritt, T.M.; Subramanian, M.A.; *MRS Bulletin*, **2006**, 31, 188. **DOI:** 10.1557/mrs2006.44.
11. Nolas, G.S.; Poon, J.; Kanatzidis, M.; *MRS Bulletin*, **2006**, 31, 199. **DOI:** 10.1557/mrs2006.45.
12. Zhou, L.; Zhang, X.; Zhao, X.; Sun, C.; Niu.; Q. *J. Alloy. Compd.*, **2010**. 502, 329. **DOI:** 10.1016/j.jallcom.2010.01.024.
13. Takashiri, M.; Miyazaki, K.; Tanaka, S.; Kurosaki, J.; Nagai, D.; Tsukamoto, H.; *J. Appl. Phys.*, **2008**, 104, 084302. **DOI:** 10.1186/s11671-015-0733-6.
14. Kim, K.T.; Choi, S.Y.; Shin, E. H.; Moon, K. S.; Koo, H.Y.; Lee, G.G.; Ha, G.H.; *Carbon*, **2013**, 52, 541. **DOI:** 10.1016/j.carbon.2012.10.008.
15. Pradhan, N.R; Duan, H.; Liang J.; Iannacchione, G.S.; *Nanotechnology.*, **2009,** 20, 245705. **DOI:** 10.1088/0957-4484/20/24/245705.
16. Smart, S.K.; Ren, W.C.; Cheng, H.M.; Lu, G. Q.; Martin, D. J.; *Int. J. Nanotechnol*., **2007,** 4, 618. **DOI:** 10.1504/IJNT.2007.014756.
17. Gao, Y.; Li, L.Y.; Tan, P.H.; Liu, L.; Zhang, Z.; *Chin. Sci. Bullet.* **2010,** 55, 3978. **DOI:** 10.1007/s11434-010-4100-9.
18. Bokobza, L.; Zhang, J.; *eXPRESS Poly. Lett.*, **2012,** 6, 601. **DOI:** 10.3144/expresspolymlett.2012.63.
19. Kaur, H.; Sharma, L.; Singh, S.; Sivaiah, B.; Reddy, G.B.; Senguttuvan, T. D.; *J. of Elect. Mater*, **2013**, 43, 1782. **DOI:** 10.1007/s11664-013-2864-9.
20. Chen, L.; Zhao, Q.; Ruan, X.; *Mater. Lett.*, **2012**, 82, 112. **DOI:** 10.1016/j.matlet.2012.04.135.

